

Article

Formation and Performance of Diamond (111)/Cu Interface from First-Principles Calculation

Yongsheng Zhao ^{1,2}, Fengyun Yan ^{1,*} and Yi An ¹

¹ State Key Laboratory of Advanced Processing and Recycling of Nonferrous Metals, Lanzhou University of Technology, Lanzhou 730050, China; zhaoyongs_2012@163.com (Y.Z.); anylut@163.com (Y.A.)

² School of Mechatronics Engineering, Lanzhou Institute of Technology, Lanzhou 730050, China

* Correspondence: yanfy@lut.edu.cn; Tel.: +86-931-2973942

Abstract: The interface formation and properties of composite materials are very important for the preparation of composite materials, and the bonding state and charge transfer between atoms in the interface have a particularly significant effect on the interface formation. In this work, the first-principles calculation method was used to study the adsorption behavior and molecular dynamics of copper atoms on the (111) surface of H-terminated diamond, and the adsorption energy and adhesion work of Cu atoms were calculated. The results show that the adsorption of copper atoms is not sensitive to the diamond (111) surface, the adsorption work is very small at the four high symmetry positions, and the adhesion work is the largest at the T4 position and is 0.6106 J/m². Furthermore, according to the electron localization function (ELF) analysis, there is no compound formation between Cu and H atoms; only a small amount of charge transfer exists, which belongs to physical adsorption. The diamond–copper interface formed by the growth of adsorption sites is a metastable structure without energy stability. This work provides an important theoretical reference for understanding the formation mechanism of copper-based diamond composites.

Keywords: composite; adsorption energies; first principles; ABINIT



Citation: Zhao, Y.; Yan, F.; An, Y. Formation and Performance of Diamond (111)/Cu Interface from First-Principles Calculation. *Coatings* **2022**, *12*, 619. <https://doi.org/10.3390/coatings12050619>

Academic Editor: Alexander Tolstoguzov

Received: 5 April 2022

Accepted: 29 April 2022

Published: 2 May 2022

Publisher's Note: MDPI stays neutral with regard to jurisdictional claims in published maps and institutional affiliations.



Copyright: © 2022 by the authors. Licensee MDPI, Basel, Switzerland. This article is an open access article distributed under the terms and conditions of the Creative Commons Attribution (CC BY) license (<https://creativecommons.org/licenses/by/4.0/>).

1. Introduction

Diamond has excellent properties such as high thermal conductivity, high hardness, wide bandgap, extremely high chemical inertness, and excellent biocompatibility due to saturated atomic bonds and stable crystal structure. It is widely used in cutting tools, composite materials, electronic devices, biosensors, and engineering fields [1–4]. Copper metal not only is a rich natural resource but also has excellent electrical conductivity, thermal conductivity, ductility, corrosion resistance, wear resistance, and other excellent properties. It is widely used in electric power, electronics, energy and petrochemical, mechanical and metallurgical, transportation, light industry, emerging industries, and other fields [5–7]. Metal matrix composites (MMCs) have been used in some necessary fields such as aerospace and microelectronics due to their better physical properties, mechanical properties, high thermal conductivity, and low thermal expansion coefficient [8,9]. Among (MMCs), diamond/Cu composites have attracted much attention due to their high thermal conductivity and low thermal expansion coefficient. Generally, before preparing diamond/Cu composites, due to the poor surface wettability of Cu and diamond, the diamond surface is pretreated by introducing Ti [10,11], W [12], Cr [13], B [14,15], Zr [16,17], Mo [18], and other vital carbon compound elements to improve the interfacial properties of copper and diamond. Then, diamond/Cu composites are prepared by vacuum (or argon protection) hot press forming, laser sintering [7], and chemical weather deposition [19]. For example, studies [12,20–22] reported that different preparation processes were used for successfully preparing copper-based diamond composites, and the thermal conductivity of 500–900 W/mK was obtained. These studies have successfully prepared copper-based

diamond composites using different processes, all of which show high thermal conductivity (TC) and low coefficient of thermal expansion (CTE). However, due to the poor wettability between copper and diamond surfaces [23] and the different preparation methods of diamond surface pretreatment and copper-based diamond composites, the micro-interface between diamond and copper has different defects such as interfacial cavities, cracks, peeling of the plating, and graphitization of the diamond surface. These defects lead to the unstable interface state between copper and diamond, and the interface between copper and diamond is essential for the thermodynamic properties and structural stability of copper-based diamond composites. Therefore, studying the formation mechanism and structural properties of the interface between copper and diamond is necessary, and it is very important to prepare copper-based diamond composites with stable properties.

The formation of the interface structure between copper and diamond is a key factor for the interface thermal conductivity and thermal resistance, also affecting the thermodynamic properties of copper-based diamond composites. The formation of the interface of copper-based diamond composites involves the behavior of adsorption, migration, and growth of copper atoms on the diamond surface. Bai et al. [15] prepared copper-based diamond composites and obtained an annular bright-field (ABF) image of the copper–diamond interface using scanning transmission electron (STE) microscopy, which clearly showed the interface structure formed between the copper (002) and the diamond (111). Scholze et al. [24], Stampfl et al. [25], and Gomez et al. [4] used first principles to calculate the diamond (111) reconstruction physical properties of the structure and the surface electronic structure and found that diamond (111) has the lowest surface energy. Larsson et al. [26] studied the diamond (111) and (100) surfaces and used H for binding to suspended carbon bonds on the surface. Levita et al. [27] studied the physical properties and chemisorption processes of water molecules on diamond (111). Xie et al. [28] investigated the interfacial structure and bonding properties of aluminum and copper atoms on diamond (111). Although these studies have explained the diamond (111) structure and the stable structure of the diamond–metal interface to a certain extent, related research on how the metal forms the interface on the diamond surface and the structure and properties of the formed interface has not been reported.

Here, based on the formation and structural properties of the diamond–Cu interface, the adsorption and interface formation behaviors of copper atoms on the surface of H-terminated diamond (111) were investigated by first principles. Furthermore, the formation mechanism of the diamond–copper interface was revealed, according to the interface adsorption energy, adhesion work, and charge density.

2. Methods and Models

2.1. Computational Details

In this work, we employed the first-principles calculations package ABINIT [29,30] based on density functional theory (DFT). The optimized norm-conserving (ONCV) pseudopotential [31] describes the interaction between ionic nuclei and valence electrons, using the generalized gradient approximation Perdew–Burke–Ernzerhof (GGA-PBE) [32] to control the exchange phase between electrons in this calculation. In the structural optimization step, the accuracy of the self-consistent loop iteration is set to 5.0×10^{-6} Ha/Bohr; the structure is considered stable when the maximum forces are smaller than 1×10^{-5} Ha/Atom. The energy cutoff (Ecut) for plane-wave basis 45 Ha is employed with a strict convergence test, and the Brillouin zones are sampled using converged $12 \times 12 \times 12$ and $4 \times 4 \times 1$ Monkhorst–Pack k-mesh grids for cells and slab structure, respectively. The effect of van der Waals force is considered in the calculation of adsorption energy. The vdW-DFT-D3 dispersion correction method was used, and the calculation convergence of van der Waals force was 1.0×10^{-12} Ha.

2.2. Electronic Properties of Cu and Diamond

In order to ensure the correct Cu and diamond crystal structures are used in the calculation, structural relaxation of the Cu and diamond crystal structures is required, and

the relaxed Cu and diamond crystal structures are shown in Figure 1. The face-centered cubic Cu single-cell structure with space group Fm-3m (225) is shown in Figure 1a. The face-centered cubic diamond single-cell structure with space group Fm-3m (227) is shown in Figure 1b, and the lattice parameters of Cu and diamond after the relaxation calculation are 3.621 Å and 3.574 Å, respectively, which are basically consistent with the experimental measurements of 3.615 Å [33] and 3.567 Å [34], indicating that the calculated values are in general agreement with the experimental data and the adopted calculation method is reliable.

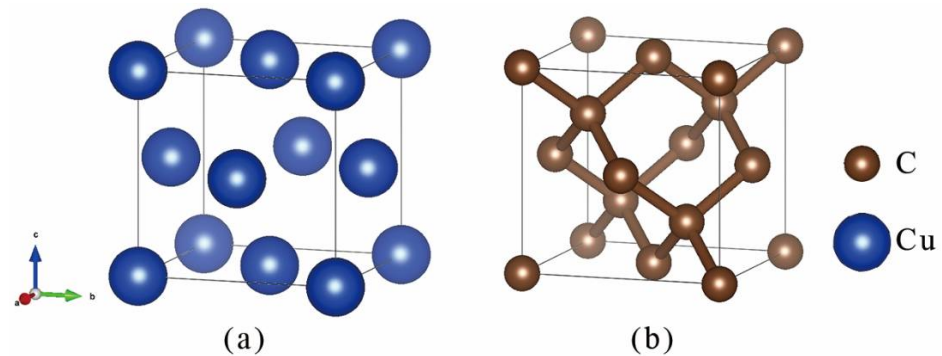


Figure 1. Crystal structures of Cu and diamond: (a) a face-centered cubic copper unit cell; (b) a face-centered cubic diamond unit cell.

The energy band structures of Cu and diamond under adiabatic conditions are shown in Figures 2 and 3, respectively. The first Brillouin zone (W-S unit cell), unique points, lines, and usual symbols of Cu and diamond protocells are shown in Figures 2a and 3a, respectively. The Monkhorst-Pack k-mesh grids of Cu and diamond for the energy band calculation are taken, and the division is performed by taking a high symmetry K-point path [35] along the Γ -X-W-K- Γ -L-U-W-L-K-U-X, shown in Figures 2a and 3a, respectively. As shown in Figure 2b, the ground state of Cu overlaps well with the Fermi surface, the valence band overlaps with the conduction band, and no bandgap exists, so its conductivity is better than that of diamond. In contrast, as shown in Figure 2b, the conduction band of a diamond is above the Fermi plane, and there is a bandgap of 4.17 eV between the bottom of the conduction band (CBM) and the top of the valence band (VBM), so diamond is an insulator.

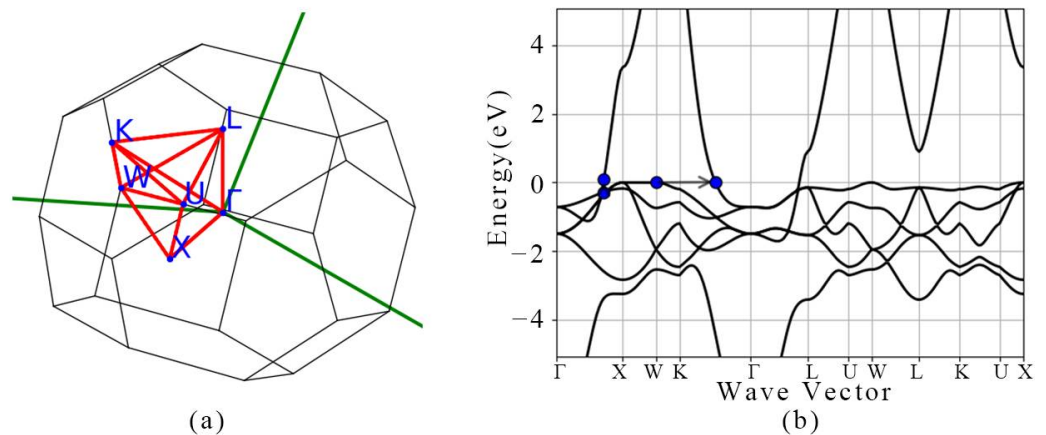


Figure 2. Band structure calculation results for Cu: (a) first Brillouin zone and K-point path; (b) energy band diagram of Cu.

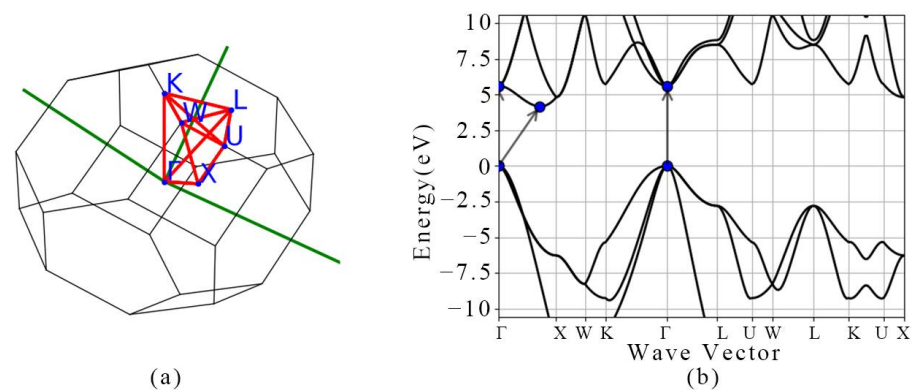


Figure 3. The energy band diagram of diamond: (a) the first Brillouin zone of diamond and the K-point path; (b) the energy band diagram of diamond.

2.3. Structure Models

Diamond (111) is considered the lowest energy and the most stable. The diamond (111) microscopic surface structure model used for the calculations in this paper was constructed by cutting after optimization of the diamond cell structure in Figure 4. The presence of carbon suspension bonds on the diamond surface leads to surface reconstruction, forming a dimer of C [36]. This is also confirmed by the graphite structure plus one obtained after optimization of the surface structure of diamond (111) without H-termination. Thus, diamond (111) is H-terminated after cutting the primitive cell. The diamond slab model (in Figure 4) contains 9 atomic lattice points and has the supercell structure of $3 \times 3 \times 7$. According to the calculated surface energy in Table 1, when the number of layers is increased to 7, the change value of surface energy is less than 0.1%. In order to ensure the calculation accuracy and improve the calculation speed, the calculated slab model contains a total of 7 layers of the diamond. The atoms of the bottom 2 layers of the slab model are fixed, and the rest are relaxed to avoid the influence of surface space on the adsorbed atoms; above the top C atoms, a vacuum layer of 15 Å is set. On the diamond (111) surface, there are four high symmetry sites according to the symmetry principle, namely Top, Br, T4, and H3 sites in Figure 4b. The Top site is indicated as perpendicular to the C atoms of the second layer directly above. The Br site is indicated as the middle of the adjacent C atoms of the surface layer directly above. The T4 site is indicated as a triple-hole site of the surface atom, directly above the sub-surface C atoms. The H3 site is indicated as another triple-hole site of the surface C atoms and is directly above the C atoms of the fourth layer.

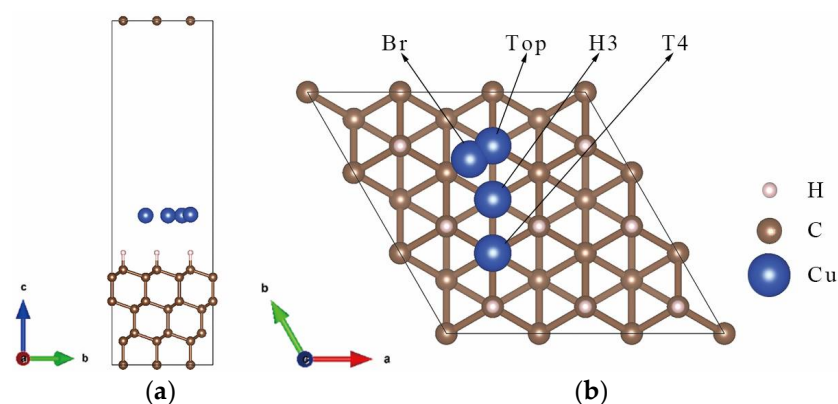


Figure 4. Slab structure model and adsorption sites of Cu atom adsorbed on the surface of H-terminated diamond (111): (a) the schematic diagram of the slab model and the adsorption point facing (100), (b) the schematic diagram of the slab model and the adsorption point facing the (001) direction. The pink balls represent H atoms, and the brown balls are C atoms. The blue balls are copper atoms.

Table 1. H-terminated diamond (111) surface 3–15 layer surface energy.

Layer (111)	E _{bulk} (eV)	E _{slab} (eV)	E _{surface} (eV/Å ²)	Layer (111)	E _{bulk} (eV)	E _{slab} (eV)	E _{surface} (eV/Å ²)
3	−507.24	−503.27	0.3588	11	−1817.47	−1813.58	0.3524
5	−834.80	−830.88	0.3540	13	−2145.03	−2141.14	0.3520
7	−1162.35	−1158.45	0.3533	15	−2472.59	−2468.70	0.3516
9	−1489.91	−1486.01	0.3529	-	-	-	-

Surface energy (E_{surf}) and adsorption energy (E_{ad}) are defined as follows:

$$E_{surf} = \frac{E_{slab} - \left(\frac{N_{slab}}{N_{bulk}}\right)E_{bulk}}{2A} \quad (1)$$

$$E_{ad} = \left(E_{surf} + NE_i - E_{tot}\right) / N \quad (2)$$

In Equation (1), E_{surf} is the free energy of the surface model. E_{slab} is the energy of the slab model. E_{bulk} is the energy of bulk lattice. N_{slab} is the number of atoms in the plate model. N_{bulk} is the number of atoms of bulk lattice. A is the surface area of the plate model.

In Equation (2), E_{ad} is the adsorption energy. E_{surf} is the free energy of the surface model. N is the number of adsorbed atoms. E_i is the single-atom energy of the adsorbed atoms. E_{tot} is the total energy of the system after atom adsorption. Surface energy is the energy required for forming surface structures by atoms inside a substance and is an essential parameter for the stability of a crystal surface.

The work of adhesion is a substantial physical quantity measuring interfacial bonding strength. A more significant value indicates greater bonding strength, defined as the reversible work done per unit area to separate an interface into two free surfaces [37]. For the diamond/copper interface system, this can be obtained from the following formulas:

$$W_{ad} = \frac{E_{diamond} + E_{Cu} - E_{tot-1}}{A} \quad (3)$$

In Equation (3), W_{ad} denotes the work of adhesion; $E_{diamond}$ and E_{Cu} denote the energy of the diamond and metal *Cu* surfaces, respectively; E_{tot-1} denotes the energy of the interface model; and A denotes the interfacial area.

3. Results and Discussion

3.1. Stiffness Matrix of Copper and Diamond Cells

The pre-calculation preparation includes parameter optimization and model validation. The parameter optimization includes the selection of surface model layers, the selection of truncation energy of *Cu* and diamond cells, and the division of the K-point grid in the Brillouin zone, as described in the calculation model section above. The elastic moduli of *Cu* and diamond play a prominent role in studying the mechanical properties of *Cu*-based diamond composites, so the elastic matrix constants of *Cu* and diamond cells were calculated separately. The Broyden–Fletcher–Goldfarb–Shanno (BFGS) method was used for structural optimization, followed by the Voigt representation to calculate the elastic stiffness constant matrices C_{ij}^{Cu} and $C_{ij}^{diamond}$ shown in Equations (4) and (5), respectively. From the calculated stiffness constant matrices, it can be seen that there are only three independent matrix elements (C_{11} , C_{12} , and C_{44}), which indicates that both *Cu* and diamond belong to the cubic crystal system, and according to Voigt–Reuss–Hill [38]

theory and equations, the elastic constants (C_{11} , C_{12} , and C_{44}) and elastic moduli (B , E , and G) of the optimized cell are verified, and the results are shown in Table 2.

$$C_{ij}^{Cu}(10^2GPa) = \begin{bmatrix} 1.8222 & 1.2839 & 1.2839 & 0 & 0 & 0 \\ 1.2839 & 1.8222 & 1.2839 & 0 & 0 & 0 \\ 1.2839 & 1.2839 & 1.8222 & 0 & 0 & 0 \\ 0 & 0 & 0 & 0.8404 & 0 & 0 \\ 0 & 0 & 0 & 0 & 0.8404 & 0 \\ 0 & 0 & 0 & 0 & 0 & 0.8404 \end{bmatrix} \quad (4)$$

$$C_{ij}^{diamond}(10^2GPa) = \begin{bmatrix} 10.4958 & 1.2285 & 1.2285 & 0 & 0 & 0 \\ 1.2285 & 10.4958 & 1.2285 & 0 & 0 & 0 \\ 1.2285 & 1.2285 & 10.4958 & 0 & 0 & 0 \\ 0 & 0 & 0 & 5.5883 & 0 & 0 \\ 0 & 0 & 0 & 0 & 5.5883 & 0 \\ 0 & 0 & 0 & 0 & 0 & 5.5883 \end{bmatrix} \quad (5)$$

Table 2. The calculation of elastic constants and elastic moduli of copper and diamond.

-	a/Å	C ₁₁ (10 ² GPa)	C ₁₂ (10 ² GPa)	C ₄₄ (10 ² GPa)	B (10 ² GPa)	E (10 ² GPa)	G (10 ² GPa)
Diamond	3.574	10.496	1.229	5.588	4.318	11.108	5.185
Ref.	3.567 [34]	10.783 [39]	1.266 [39]	5.774 [39]	4.442 [39]	11.43 [40]	5.35 [39]
Cu	3.621	1.822	1.284	0.84	1.463	1.426	0.533
Ref. [41]	-	1.807	1.091	0.754	-	1.14	-

The calculated results of elastic properties of bulk Cu and bulk diamond are listed in Table 2. The bulk modulus (B), Young’s modulus (E), and shear modulus (G) of Cu are lower than those of diamond. In particular, Young’s modulus E , which is 1110.8 Gpa for diamond and 142.6 Gpa for Cu, indicates that the deformation resistance of diamond is much higher than that of the Cu structure, and the diamond stiffness is stronger. However, since the shear modulus G of diamond is 518.5 Gpa, which is greater than that of Cu at 53.3 Gpa, this also indicates that the plasticity of Cu is more robust than that of diamond.

3.2. Adsorption of a Single Cu Atom

For transition-zone-free interfaces, which consist of only a few atomic layers, the adsorption of individual atoms significantly influences the formation and structure of the interface. According to the geometric structure analysis, the leading high symmetry positions on the surface of diamond (111) are Top, Br, H3, and T4 positions (shown in Figure 4). In order to determine the stable adsorption positions of the Cu atom on the H-terminated diamond (111) surface, the adsorption distances of the Cu atom were first determined in the adiabatic state, then the adsorption energies of the above high symmetry positions were compared in the relaxed state of C atoms on the surface, as shown in Table 3.

Table 3. A single Cu atom’s adsorption energy and adhesion work on different adsorption sites on a diamond (111) surface.

-	Top	T4	H3	Br
E_{tot} (eV)	−15,585.1000	−15,585.1039	−15,585.1032	−15,585.1034
E_{ad} (eV)	0.2069	0.2108	0.2102	0.2103
E_{ad}^* (eV)	0.3279	0.3344	0.3287	0.3289
W_{ad} (J/m ²)	0.5994	0.6106	0.6088	0.6092

E_{ad}^* (eV) is the adsorption energy considering the van der Waals force.

The adsorption energies and work of adhesion are listed in Table 3, the adsorption energies of a single Cu atom on the H-terminated diamond (111) surface are all low. The

adsorption energy at the T4 position is 0.2108 eV, and the work of adhesion is 0.6106 J/m². Both the adsorption energy and the work of adhesion are the highest among the four spots. The difference in adsorption energy and the work of adhesion between the four adsorption spots is not significant, with a maximum difference of 0.0112 eV and 0.0112 J/m², respectively. When the van der Waals force is considered, the adsorption energy of Cu atoms becomes bigger, but the effect of this change on the four positions is almost the same. That is, the analysis of the adsorption positions is the same. Since there is a weak interaction between Cu atoms and the H-terminated diamond surface, and the van der Waals force is an overall effect, the influence on adsorption and interface structure remains unchanged, so the following calculations will not be discussed.

3.3. Diamond (111)/Cu Interface Performance

In order to analyze the surface charge distribution at the four sites after structural relaxation and the bonding between the diamond (111) surface and Cu atoms, the charge density maps of the four adsorption sites (crystal orientation 100 direction) were made separately, as shown in Figure 5. The distances between Cu atoms and the nearest neighboring H atoms are 2.467, 2.811, 2.812, and 2.645 Å when a single Cu atom is adsorbed at the Top, T4, H3, and Br adsorption sites, respectively. In contrast, the distances between the H atoms and the C atoms are 1.117, 1.111, 1.111, and 1.113 Å, respectively. Furthermore, the C-H bond length before comparative relaxation is 1.107 Å, so when the surface of diamond (111) adsorbs Cu atoms, the C-H bonds grow to different degrees, which also shows a weak force between the Cu atom and the surface H atoms.

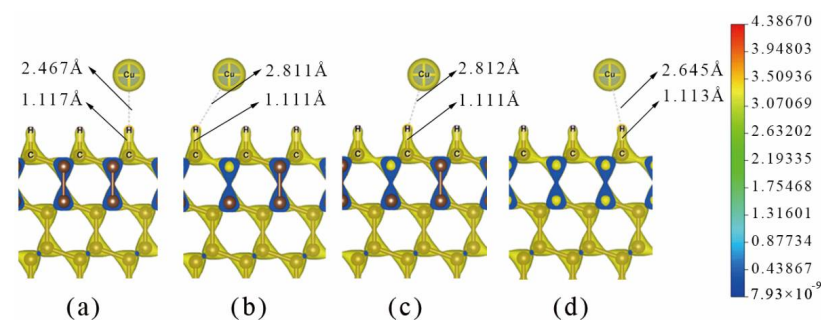


Figure 5. (a–d) Charge density maps of a single Cu atom adsorbed on the Top, T4, H3, and Br adsorption sites, respectively.

As shown from the charge density diagram in Figure 5, ionic bonds are formed between C and H atoms on the surface, while the C–C bonds inside the diamond show a transparent tetrahedral distribution between them. That thus leads to saturated C–H bonds on the surface, making it impossible for the adsorbed Cu atom to form other forms of interactions with C and H atoms, which can only exist in the form of physical adsorption on the diamond (111) surface.

While the charge density can also partially reflect the charge transfer between Cu–H bonds, to analyze the bonding state and charge transfer between Cu atoms and H-terminated diamond (111) surfaces, electron localization function (ELF) calculation was performed on the four highly symmetric adsorption models. The calculation results are shown in Figure 6. It should be noted here that the value of ELF is between 0 and 1. The upper limit of 1 indicates that the electrons are completely localized, while the value of 0 may indicate that the electrons are completely delocalized. Taking the intermediate value indicates that the electrons form electrons similar to an electron gas pair distribution. It can be seen from Figure 6 that the ELF values of the Cu atoms in the four highly symmetrical positions are 1, the ELF values of the C–H bonds are between 0.69 and 0.78, and the ELF values of the C–C bonds are about 0.5. In addition, we can see in Figure 6 that the Cu atoms on the four highly symmetric adsorption sites are all displayed in bright red, which indicates that the electron distribution on the Cu atoms is highly localized, which is also consistent

with the properties of the Cu atoms belonging to d-state metals. The upper end of the H atom on the diamond (111) surface shows a light yellow color, indicating that the electrons in the C–H bonds have deviated, which also proves that the C–H bonds on the diamond (111) surface are polar bonds. The fundamental reason is that the electronegativities of H atoms and C atoms are different. In contrast, electrons on C–C bonds in diamond exhibit an approximate electron gas distribution.

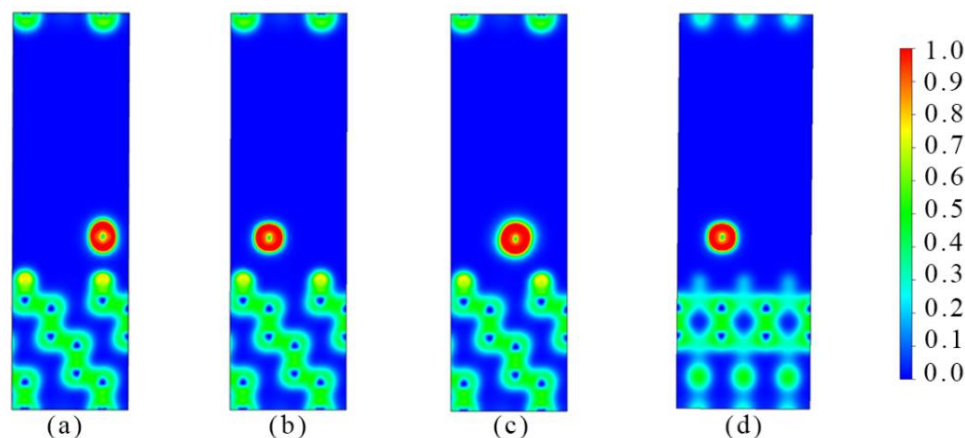


Figure 6. The 2D-ELF section views of four highly symmetric adsorption sites, where (a–d) show the Top, T4, H3, and Br adsorption sites, respectively.

In summary, Cu atoms mainly exist in the form of physical adsorption on the surface of diamond (111) terminated by H. The weak adsorption energy and smooth potential energy surface are beneficial to forming the lowest energy structure by simple migration of Cu atoms. Therefore, the Cu atoms are not sensitive to the H-terminated diamond (111) surface. According to the adhesion work formed by the four adsorption sites calculated in Table 3, the adhesion work values of the four adsorption sites are all greater than 0, which indicates that the Cu atoms are theoretically stable on the H-terminated diamond (111) surface. The interfacial adhesion work at the T4 position is the largest at 0.6106 J/m^2 , and the adhesion work at the Top position is the minimum at 0.5994 J/m^2 . Even though a single Cu atom can form stable adsorption on the H-terminated diamond (111) surface, when the Cu atom fills the entire surface, due to the fluctuation of the surface potential, it will make the interface between diamond (111) and Cu exist in a metastable state. Since the adhesion work values of Cu atoms on the four adsorption sites on the diamond (111) surface are around 0, the stability of the interface is easily destroyed due to changes in the external environment, such as the preparation of copper-based diamond composites. Furthermore, the high temperature will increase the atomic kinetic energy, making it exceed the adhesion work of the interface, forming a non-wetting interface.

According to the above predictions, the molecular dynamics simulation of the diamond (111)/Cu (200) interface was performed using the NVT (number of particles (N), volume (V), and temperature (T)) method, using NVT molecular dynamics due to the fact that it is closer to the processing technology of copper-based diamond composites using hot pressing. The ion time steps are 2.5 fs, the maximum number of molecular dynamics time steps is 100, the simulation temperature is 1223 K [15], and the simulation process fixes the bottom two layers of C atoms and the top two layers of Cu atoms. The simulation results can be seen in Figure 7.

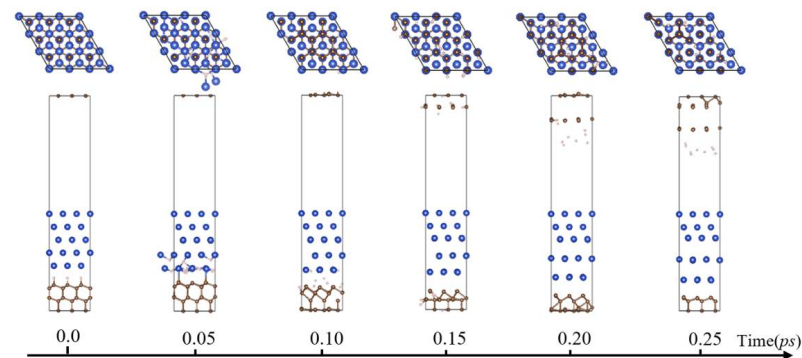


Figure 7. Molecular dynamics simulation of diamond (111)/Cu (200) interface.

At high temperature, the H atoms on the diamond surface are detached from the surface C atoms and combined with part of the bottom Cu atoms. With the continuous detachment of the H atoms on the diamond surface, the diamond surface begins to graphitize. After all the H atoms “escape” to the vacuum layer, the diamond surface is compressed, and the C atoms, after graphitization of the surface layer, gradually move downward. This process is accompanied by the decline in Cu atoms at the interface. When some C atoms on the diamond surface “escape” to the vacuum layer, the interface between diamond and Cu is basically in a stable state. Since the simulation temperature is 1223 K, this temperature is not enough to melt diamond and Cu, but it is enough to graphitize the diamond surface, which is consistent with the experimental phenomenon observed by Bai et al. [15].

A small number of interatomic interaction forces exist at the unstable diamond (111)/Cu (200) interface. In the density of states projection diagram (DOS) shown in Figure 8, the Fermi level is in the interval with a DOS value of 0 and a gap of 2.26 eV. From the partial density of states (PDOS) plot shown in Figure 9, it can be seen that in the s orbital, there are hybrid resonance peaks in some orbitals between H atoms and C atoms. This phenomenon indicates the formation of chemical bonds between H atoms and C atoms, consistent with the results in Figure 6. The results are consistent with the formation of chemical bonds. On the p orbital, there is a small hybrid resonance peak between the surface C atoms, H atoms, and Cu atoms, indicating a weak charge transfer between the surface C, H, and Cu atoms, but no chemical bonds are formed. The Cu atoms in the d orbital show robust localization, and a prominent peak appears. Its corresponding energy band is narrow, consistent with Cu’s nature as a metal element in the d region.

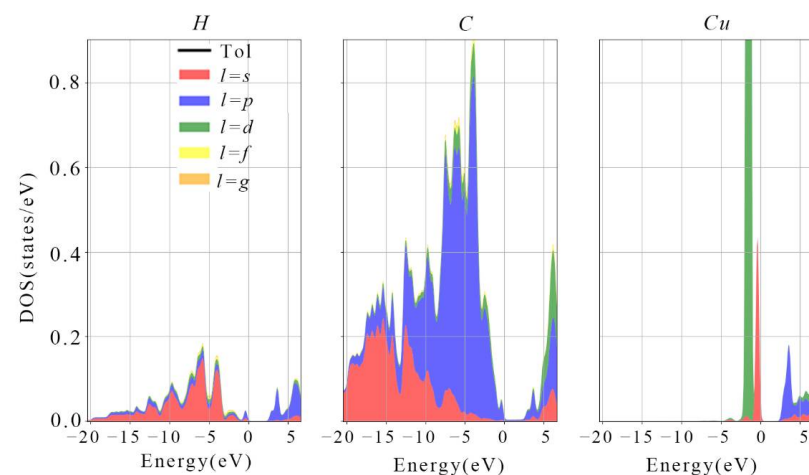


Figure 8. H, C, and Cu atomic DOS map of the copper–diamond interface, 0 points can represent the Fermi level.

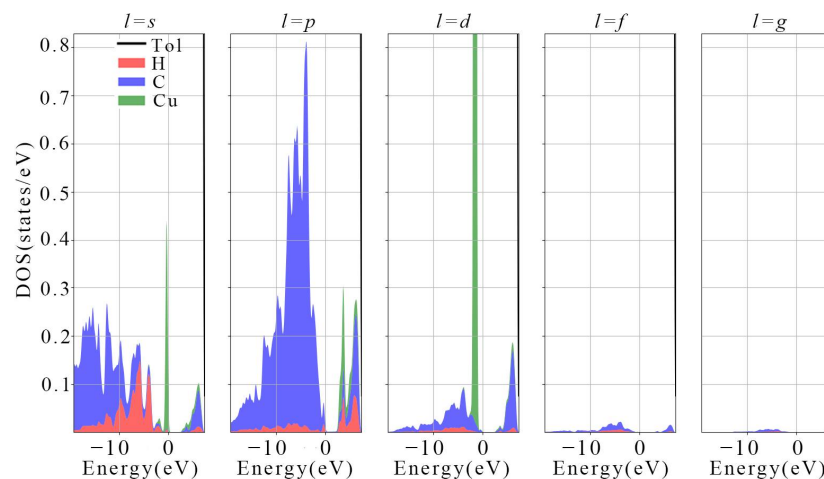


Figure 9. T4 point PDOS map, 0 points can represent the Fermi level.

4. Conclusions

In this paper, the adsorption behavior of a single Cu atom on the H-terminated diamond (111) surface was systematically calculated through first principles. The molecular dynamics simulation of the diamond (111)/Cu (200) interface was performed by using the NVT method. The conclusions drawn are as follows:

- (1) Cu atoms are not sensitive to the H-terminated diamond (111) surface structure. The adsorption energy and adhesion work of the four high symmetry positions are almost the same, with a maximum difference of 0.0039 eV. When the van der Waals force is considered, the adsorption energy at the four sites increases, and the effect on the interface structure remains unchanged.
- (2) By analyzing the ELF's and atomic distances of the four high symmetry sites, it was found that no chemical bonds were formed between Cu and H atoms, and there was only a small charge transfer. Cu atoms are physically adsorbed on the surface of H-terminated diamond (111).
- (3) The diamond (111) surface will be graphitized, and a small part of the surface C atoms will escape into the Cu atoms. The bottom Cu atoms will move downward.

The above results provide an important theoretical reference for understanding the formation mechanism of the diamond/Cu interface in the preparation of copper-based diamond composites.

Author Contributions: Y.Z.: conceptualization, methodology, formal computing, manuscript writing and editing, project management. F.Y.: project management, supervision. Y.A.: data analysis, model building. All authors have read and agreed to the published version of the manuscript.

Funding: This research was funded by the Education Department of Gansu Province, grant number 2021B-310, and the Lanzhou Institute of Technology, grant number 2020KJ-17.

Institutional Review Board Statement: Not applicable.

Informed Consent Statement: Not applicable.

Data Availability Statement: The datasets generated during or analyzed during the current study are available from the corresponding author on reasonable request.

Conflicts of Interest: The authors have no relevant financial or non-financial interest to disclose.

References

1. Zhang, X.-Y.; Xu, M.; Cao, S.-Z.; Chen, W.-B.; Yang, W.-Y.; Yang, Q.-Y. Enhanced thermal conductivity of diamond/copper composite fabricated through doping with rare-earth oxide Sc_2O_3 . *Diam. Relat. Mater.* **2020**, *104*, 107755. [[CrossRef](#)]
2. Jia, J.; Bai, S.; Xiong, D.; Wang, J.; Chang, J. Effect of tungsten based coating characteristics on microstructure and thermal conductivity of diamond/Cu composites prepared by pressueless infiltration. *Ceram. Int.* **2019**, *45*, 10810–10818. [[CrossRef](#)]

3. Liu, Z.; Zheng, S.; Lu, Z.; Pu, J.; Zhang, G. Adhesive transfer at copper/diamond interface and adhesion reduction mechanism with fluorine passivation: A first-principles study. *Carbon* **2018**, *127*, 548–556. [[CrossRef](#)]
4. Gomez, H.; Groves, M.; Neupane, M. Study of the structural phase transition in diamond (100) & (111) surfaces. *Carbon Trends* **2021**, *3*, 100033. [[CrossRef](#)]
5. Pan, Y.; He, X.; Ren, S.; Wu, M.; Qu, X. Optimized thermal conductivity of diamond/Cu composite prepared with tungsten-copper-coated diamond particles by vacuum sintering technique. *Vacuum* **2018**, *153*, 74–81. [[CrossRef](#)]
6. Soltani, H.M.; Tayebi, M. Determination of wear parameters and mechanisms of diamond/copper tools in marble stones cutting. *Int. J. Refract. Met. Hard Mater.* **2020**, *87*, 105172. [[CrossRef](#)]
7. Pillari, L.K.; Bakshi, S.R.; Chaudhuri, P.; Murty, B. Fabrication of W-Cu functionally graded composites using high energy ball milling and spark plasma sintering for plasma facing components. *Adv. Powder Technol.* **2020**, *31*, 3657–3666. [[CrossRef](#)]
8. Raza, K.; Khalid, F.A. Optimization of sintering parameters for diamond-copper composites in conventional sintering and their thermal conductivity. *J. Alloy. Compd.* **2014**, *615*, 111–118. [[CrossRef](#)]
9. Cuevas, A.C.; Becerril, E.B.; Martínez, M.S.; Ruiz, J.L. *Metal Matrix Composites*; Springer: Cham, Switzerland, 2018. [[CrossRef](#)]
10. Che, Q.; Chen, X.; Ji, Y.; Li, Y.; Wang, L.; Cao, S.; Jiang, Y.; Wang, Z. The influence of minor titanium addition on thermal properties of diamond/copper composites via in situ reactive sintering. *Mater. Sci. Semicond. Process.* **2015**, *30*, 104–111. [[CrossRef](#)]
11. Li, J.; Zhang, H.; Wang, L.; Che, Z.; Zhang, Y.; Wang, J.; Kim, M.J.; Wang, X. Optimized thermal properties in diamond particles reinforced copper-titanium matrix composites produced by gas pressure infiltration. *Compos. Part A Appl. Sci. Manuf.* **2016**, *91*, 189–194. [[CrossRef](#)]
12. Abyzov, A.M.; Kidalov, S.V.; Shakhov, F.M. High thermal conductivity composite of diamond particles with tungsten coating in a copper matrix for heat sink application. *Appl. Therm. Eng.* **2012**, *48*, 72–80. [[CrossRef](#)]
13. Liu, X.; Sun, F.; Wang, L.; Wu, Z.; Wang, X.; Wang, J.; Kim, M.J.; Zhang, H. The role of Cr interlayer in determining interfacial thermal conductance between Cu and diamond. *Appl. Surf. Sci.* **2020**, *515*, 146046. [[CrossRef](#)]
14. Bai, G.; Li, N.; Wang, X.; Wang, J.; Kim, M.J.; Zhang, H. High thermal conductivity of Cu-B/diamond composites prepared by gas pressure infiltration. *J. Alloy. Compd.* **2018**, *735*, 1648–1653. [[CrossRef](#)]
15. Bai, G.; Wang, L.; Zhang, Y.; Wang, X.; Wang, J.; Kim, M.J.; Zhang, H. Tailoring interface structure and enhancing thermal conductivity of Cu/diamond composites by alloying boron to the Cu matrix. *Mater. Charact.* **2019**, *152*, 265–275. [[CrossRef](#)]
16. He, J.; Wang, X.; Zhang, Y.; Zhao, Y.; Zhang, H. Thermal conductivity of Cu-Zr/diamond composites produced by high temperature-high pressure method. *Compos. Part B Eng.* **2015**, *68*, 22–26. [[CrossRef](#)]
17. Wang, L.; Li, J.; Bai, G.; Li, N.; Wang, X.; Zhang, H.; Wang, J.; Kim, M.J. Interfacial structure evolution and thermal conductivity of Cu-Zr/diamond composites prepared by gas pressure infiltration. *J. Alloy. Compd.* **2019**, *781*, 800–809. [[CrossRef](#)]
18. Kang, Q.; He, X.; Ren, S.; Zhang, L.; Wu, M.; Guo, C.; Liu, Q.; Liu, T.; Qu, X. Effect of molybdenum carbide intermediate layers on thermal properties of copper-diamond composites. *J. Alloy. Compd.* **2013**, *576*, 380–385. [[CrossRef](#)]
19. Sun, F.; Feng, J.; Li, D. Bonding of CVD diamond thick films using an Ag-Cu-Ti brazing alloy. *J. Mater. Process. Technol.* **2001**, *115*, 333–337. [[CrossRef](#)]
20. Lei, L.; Bolzoni, L.; Yang, F. High thermal conductivity and strong interface bonding of a hot-forged Cu/Ti-coated-diamond composite. *Carbon* **2020**, *168*, 553–563. [[CrossRef](#)]
21. Arai, S.; Ueda, M. Fabrication of high thermal conductivity copper/diamond composites by electrodeposition under potentiostatic conditions. *J. Appl. Electrochem.* **2020**, *50*, 631–638. [[CrossRef](#)]
22. Sun, H.; Guo, L.; Deng, N.; Li, X.; Li, J.; He, G.; Li, J. Elaborating highly thermal-conductive diamond/Cu composites by sintering intermittently electroplated core-shell powders. *J. Alloy. Compd.* **2019**, *810*, 151907. [[CrossRef](#)]
23. Wu, M.; Chang, L.; Zhang, L.; He, X.; Qu, X. Wetting mechanism of AgCuTi on heterogeneous surface of Diamond/Cu composites. *Surf. Coatings Technol.* **2017**, *325*, 490–495. [[CrossRef](#)]
24. Scholze, A.; Schmidt, W.; Käckell, P.; Bechstedt, F. Diamond (111) and (100) surface: Ab initio study of the atomic and electronic structure. *Mater. Sci. Eng. B* **1996**, *37*, 158–161. [[CrossRef](#)]
25. Stampfl, C.; Derry, T.; Makau, N.W. Interaction of diamond (111)-(1 × 1) and (2 × 1) surfaces with OH: A first principles study. *J. Phys. Condens. Matter* **2010**, *22*, 475005. [[CrossRef](#)]
26. Larsson, K. The Combined Influence of Dopant Species and Surface Termination on the Electronic Properties of Diamond Surfaces. *C* **2020**, *6*, 22. [[CrossRef](#)]
27. Levita, G.; Kajita, S.; Righi, M. Water adsorption on diamond (111) surfaces: An ab initio study. *Carbon* **2018**, *127*, 533–540. [[CrossRef](#)]
28. Xie, H.; Chen, Y.; Zhang, T.; Zhao, N.; Shi, C.; He, C.; Liu, E. Adhesion, bonding and mechanical properties of Mo doped diamond/Al (Cu) interfaces: A first principles study. *Appl. Surf. Sci.* **2020**, *527*, 146817. [[CrossRef](#)]
29. Gonze, X.; Amadon, B.; Antonius, G.; Arnardi, F.; Baguet, L.; Beuken, J.-M.; Bieder, J.; Bottin, F.; Bouchet, J.; Bousquet, E.; et al. The Abinitproject: Impact, environment and recent developments. *Comput. Phys. Commun.* **2020**, *248*, 107042. [[CrossRef](#)]
30. Romero, A.H.; Allan, D.C.; Amadon, B.; Antonius, G.; Applencourt, T.; Baguet, L.; Bieder, J.; Bottin, F.; Bouchet, J.; Bousquet, E.; et al. ABINIT: Overview and focus on selected capabilities. *J. Chem. Phys.* **2020**, *152*, 124102. [[CrossRef](#)]
31. Hamann, D.R. Optimized norm-conserving Vanderbilt pseudopotentials. *Phys. Rev. B* **2013**, *88*, 085117. [[CrossRef](#)]
32. Perdew, J.P.; Burke, K.; Ernzerhof, M. Generalized gradient approximation made simple. *Phys. Rev. Lett.* **1996**, *77*, 3865. [[CrossRef](#)] [[PubMed](#)]

33. Straumanis, M.E.; Yu, L.S. Lattice parameters, densities, expansion coefficients and perfection of structure of Cu and of Cu-In α phase. *Acta Crystallogr. Sect. A* **1969**, *25*, 676–682. [[CrossRef](#)]
34. Hom, T.; Kiszenik, W.; Post, B. Accurate lattice constants from multiple reflection measurements. II. Lattice constants of germanium silicon, and diamond. *J. Appl. Crystallogr.* **1975**, *8*, 457–458. [[CrossRef](#)]
35. Rao, L.; Liu, H.; Shao, W.; Hu, T.; Xing, X.; Ren, J.; Zhou, Y.; Yang, Q. Investigation on the interface characteristic between TiN and diamond by first-principles calculation. *Diam. Relat. Mater.* **2020**, *109*, 108023. [[CrossRef](#)]
36. Feng-Bin, L.; Jia-Dao, W.; Da-Rong, C.; Ming, Z.; Guang-Ping, H. The microstructures of the diamond (100) surfaces with different density of hydrogen adsorption. *Acta Phys. Sin.* **2010**, *59*, 6556–6562. [[CrossRef](#)]
37. Siegel, D.; Hector, L.G.; Adams, J.B. First-principles study of metal-carbide/nitride adhesion: Al/VC vs. Al/VN. *Acta Mater.* **2002**, *50*, 619–631. [[CrossRef](#)]
38. Man, C.-S.; Huang, M. A Simple Explicit Formula for the Voigt-Reuss-Hill Average of Elastic Polycrystals with Arbitrary Crystal and Texture Symmetries. *J. Elast.* **2011**, *105*, 29–48. [[CrossRef](#)]
39. Migliori, A.; Ledbetter, H.; Leisure, R.G.; Pantea, C.; Betts, J.B. Diamond's elastic stiffnesses from 322 K to 10 K. *J. Appl. Phys.* **2008**, *104*, 053512. [[CrossRef](#)]
40. Klein, C.A.; Cardinale, G.F. Young's modulus and Poisson's ratio of CVD diamond. *Diam. Relat. Mater.* **1993**, *2*, 918–923. [[CrossRef](#)]
41. Ichitsubo, T.; Tane, M.; Ogi, H.; Hirao, M.; Ikeda, T.; Nakajima, H. Anisotropic elastic constants of lotus-type porous copper: Measurements and micromechanics modeling. *Acta Mater.* **2002**, *50*, 4105–4115. [[CrossRef](#)]